Magnetic Model Calibration for Tetherless Surgical Needle Manipulation using Zernike Polynomial Fitting

Suraj Raval[1]*, Onder Erin[2], Xiaolong Liu[2], Lamar O. Mair[3], Will Pryor[4], Yotam Barnoy[4], Irving N. Weinberg[3], Axel Krieger[2], and Yancy Diaz-Mercado[1]

2021 IEEE 21st International Conference on Bioinformatics and Bioengineering (BIBE) | 978-1-6654-4261-9/21/$31.00 ©2021 IEEE | DOI: 10.1109/BIBE52308.2021.9635512

***Abstract*— Exerting forces and torques instantaneously on rigid magnetic bodies with no physical connection is an attractive feature of magnetic robotics. This demonstrates great potential for manipulating tools that are externally controlled through the use of magnetic fields in minimally invasive surgeries. The magnetic field can be controlled by the application of currents to electromagnets positioned around the surgical site, and the necessary currents for a specific desired manipulation can be derived from magnetic field models. However, the magnetic field generated by electromagnetic coils are highly nonlinear, especially in the vicinity of the magnetic field sources, which complicates the modeling process. While simple dipole models provide a good approximation for these fields far away from the electromagnets, these models tend to be highly inaccurate near the sources. Magnetic surgical applications benefit from models which accurately describe fields and gradients both near and far from the field source. Particularly, since forces and torques decay inversely proportionally with the cube of the distance to the coil, inaccurate modeling near the coil makes large regions near the coil unfit for applications requiring precisely predicted motion. Estimation errors near coils generate inaccuracies in field models that significantly reduce control performance for rigid magnetic bodies. In order to tackle this problem, we utilize Zernike basis functions to analytically represent the nonlinear magnetic field distribution more accurately. The accuracy of the controller is tested experimentally by driving a magnetic surgical suture needle with a length of 22 mm in the MagnetoSuture™ system along a lemniscate trajectory. The magnetic needle's tip position and the needle orientation, autonomously controlled by the proposed controller, shows RMS tracking error of 2.35 mm using typical dipole models and 1.71 mm for the Zernike fitting approach, a 27% improvement in tracking error. This suggests that the use of Zernike basis functions to capture the nonlinearities of the magnetic field may assist in implementing fast and precise autonomous control strategies for magnetic suture needles.**

***Index Terms*— Magnetic Manipulation; Autonomous Control; Medical Robotics; Zernike Polynomials**

This paper was supported by the University of Maryland Medical Device Development Fund (MDDF) and the National Institute of Biomedical Imaging and Bioengineering (NIBIB) of the National Institutes of Health under award number R01EB020610.

* Corresponding author: sraval@umd.edu

[1]Authors are with the Department of Mechanical Engineering, University of Maryland, College Park, MD 20742, USA.

[2]Authors are with the Department of Mechanical Engineering, Johns Hopkins University, Baltimore, MD 21218, USA.

[3]Authors are with the Division of Magnetic Manipulation & Particle Research, Weinberg Medical Physics, Inc., North Bethesda, MD 20852, USA.

[4]Authors are with the Department of Computer Science, Johns Hopkins University, Baltimore, MD 21218, USA.

I. Introduction

Advancing autonomous control of surgical tools may enable minimally invasive surgeries (MIS) to become less invasive, require fewer incisions, enable faster recovery, and further reduce the cosmetic implications of some interventions [1]. While endoscopy and laparoscopy have reduced the invasiveness of surgical procedures in the gastrointestinal (GI) tract and abdomen, most surgical tools require physically contacting surgical tools with manipulators, necessitating multiple portals from outside to inside the patient [2]–[4]. The size and number of instruments for contact manipulation of surgical tools present barriers to achieving ultra minimally invasive surgeries (u-MIS) that may be performed via untethered manipulation of a surgical tool such as a suture needle. Magnetic robotics provides a useful alternative to contact manipulation by allowing remote force and torque exertion to magnetic tools [5]. Such untethered manipulation methods may allow further miniaturization of overall surgical apparatus and decrease the number of incisions, moving some procedures closer to u-MIS status. However, to use these, extremely fine control over surgical tool pose and applied force must be accomplished.

Several approaches for magnetic manipulation exist [6]–[8]. Manipulation of magnetic objects via (1) orienting/rotating with magnetic fields and (2) using magnetic gradients offer two approaches, each with various strengths and weaknesses. Uniform, rotating magnetic manipulation methods spin, roll, or twist magnetic robots and have been well-modeled, allow for precise positioning of various robots, and offer a broad range of rotating frequencies [9]–[18]. Magnetic gradient pulling obviates the need for the robot to have helical shape, but poses challenges in force and controllability due to spatial variation in the magnetic gradient, and the fact that robot motion is tightly coupled to the gradient with increasing gradient resulting in increasing robot velocity [19]–[21]. Thus, the gradient pulling method presents a double edged sword: While it allows for manipulation of broad classes of magnetic surgical tools, it requires strong gradients for clinical operations in practical settings. Additionally, gradient pulling requires fast feedback rates and an accurate controller so as to avoid motion irregularities. As such, gradient pulling of magnetic surgical tools has often been considered comparatively unstable and challenging to control, particularly near magnetic field sources.

For magnetic robot manipulation near coils, commonly

employed magnetic dipole models are not accurate enough to provide precise control. A complete estimation of the forces and torques on the magnet can be achieved by finite element models (FEM), which consider both the electromagnet and the needle magnetization, volume, and shape. However, such computations are time consuming for autonomous control purposes, where real-time feedback is required for efficient and practical computation of control signals. To find a solution to the nonlinear magnetic field distribution that is sufficiently fast and efficient to enable safe, precise, and autonomous control of surgical magnetic robots, we approximate the nonlinear magnetic field by a linear combination of nonlinear basis functions, similar to the approach taken in [22]. Our approach differs in that the approximation is accomplished by using a small number of Zernike polynomials [23] to fit the FEM data. Zernike polynomials are widely used to characterize wavefronts in optics [24], [25]. However, their rotational symmetry properties provide sufficiently rich features to also capture the magnetic field characteristics in a local region near a coil using only a few terms. Improvement in accuracy is demonstrated on the MagnetoSuture™ system shown in Fig. 4, which utilizes current control to generate magnetic fields that steer a magnetic suture needle along a reference path in real time using localization from an overhead camera [26], [27]. Here, we focus on advancing magnetic pulling-based needle control via optimization of Zernike polynomial fitting, as demonstrated via manipulation of a suture needle steered along a complex path.

The primary contributions of this paper include: 1) generating a set of Zernike basis functions that provide an analytic estimate of the field near an electromagnetic coil array; and 2) experimental validation of these estimates via improved suture needle tip-tracking in real time, as compared with a simple dipole model-based controller.

The paper is organized as follows: Section II provides background information on how magnetic fields induce forces and torques on magnetic objects. Section III introduces the Zernike polynomials. Section IV describes analysis for FEM-based approximations of magnetic fields. Section V presents the MagnetoSuture™ experimental testbed and the motion control performance. Conclusions are provided in Section VI.

II. Magnetic Forces and Torques

Let the magnetic vector field induced by a current-carrying coil be given by B. If a magnet with magnetic moment vector m_p is present in the external magnetic field generated by this coil, the force applied on the magnet is equivalent to the gradient of the magnetic potential

$$F = \nabla(m_p \cdot B). \tag{1}$$

The torque on the magnet is given by

$$\tau = m_p \times B. \tag{2}$$

When the magnetic field is generated by a current-carrying coil that is relatively small and sufficiently far away, it can

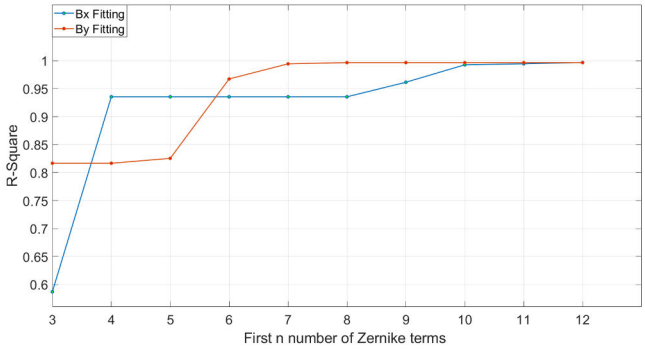

Fig. 1: Change in R^2 value in relation to number of Zernike terms used for fitting the magnetic field contours.

be approximated using a dipole model, i.e.,

$$B_{dipole}(d) = -\frac{\mu_0}{4\pi\|d\|^3}\left(I - 3\frac{dd^T}{\|d\|^2}\right)m_e, \tag{3}$$

where d is the displacement vector from the center of the coil, and m_e is the magnetic moment vector of the coil, proportional to the current.

Although the dipole model gives a suitable approximation of the magnetic field B at far away distances, it does not capture the nonlinearities at locations near to the coil. Thus, we will introduce through the principle of superposition a set of terms that can capture these nonlinearities. These terms more accurately model the magnetic field, even for near-field calculations.

III. The Zernike Basis

Zernike polynomials were originally formulated in order to characterize the diffracted wavefront in phase contrast imaging. Typical applications of these polynomials are in ophthalmic optics and optical testing, where the polynomials are used to fit complex and non-rotationally symmetric surfaces over a circular domain.

Zernike polynomials form a complete basis with two variables, a radial component ρ and angular component θ, that are orthogonal in a continuous manner over a unit circle. These polynomials are separable, and can be expressed as products of radial and angle functions. They can be even or odd. Even Zernike polynomials can be expressed as

$$Z_n^m(\rho,\theta) = R_n^m(\rho)\cos(m\theta), \tag{4}$$

while odd Zernike polynomials can be represented as

$$Z_n^{-m}(\rho,\theta) = R_n^m(\rho)\sin(m\theta). \tag{5}$$

where θ is the azimuth angle, m and n are non-negative integers with $0 \le m \le n$, and ρ is the radial distance with $0 \le \rho \le 1$. The radial polynomials R_n^m can be expressed as

$$R_n^m(\rho) = \sum_{i=0}^{\frac{n-m}{2}} \frac{(-1)^i(n-i)!}{i!\,(\frac{n+m}{2}-i)!\,(\frac{n-m}{2}-i)!}\rho^{n-2i}.$$

The derivatives of these Zernike terms can be readily obtained in closed form, which is helpful for representing the resultant forces acting on the magnet, as these are given by the gradients of the magnetic field.

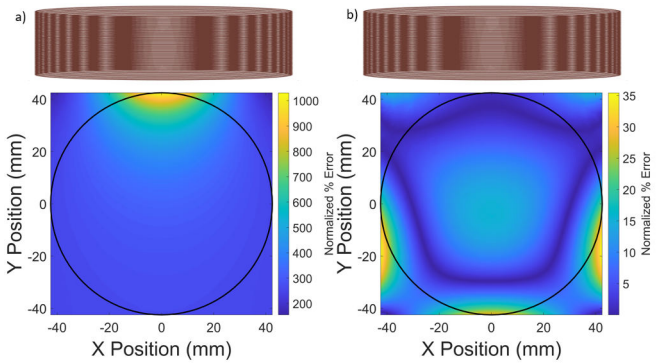

Fig. 2: Normalized percentage error between the FEM and the (a) dipole model and (b) Zernike fitting with four terms per component, for the magnetic field generated from the north coil with 1A current.

IV. Magnetic Field FEM and Zernike Basis Fit

The magnetic field FEM was generated by using COMSOL Multiphysics® V5.6 along the Cartesian directions shown in Fig. 4. The magnetic field is produced from an electromagnet (coil along the positive y-axis) activated by 1 A current. The region of interest is a circular petri-dish 85 mm in diameter ($R_{dish} = 42.5$ mm). We generated approximately 29,000 data points in a grid of equidistant points at 0.5 mm in Cartesian directions for each component of magnetic field, inside a square of side $2R_{dish}$.

We use the Zernike basis functions to fit the FEM contour plots for B_x and B_y separately. The number of Zernike terms to be chosen depends on the tolerable error in fitting as well as on the speed of computation of these functions for real-time implementation on our MagnetoSuture™ system. The graph in Fig. 1 represents the change in R^2 (coefficient of determination) value with addition of more Zernike terms. The figure shows diminishing returns in fitting accuracy as the number of terms is increased beyond the first few Zernike polynomials. Further, studying the shapes of Zernike terms individually can help us eliminate unnecessary terms before starting the fitting process. Here we use $\ell = 4$ different terms to approximate each of the B_x and B_y contours.

Consider m identical electromagnetic coils. The centers for these are uniformly spaced around a dish at positions $r_i \in \mathbb{R}^2$, which are a fixed radius ($\|r_i\| = 80mm$) and varying angles $\theta_i = 2\pi((i-1)/m)$ from the origin (center of dish). The centerlines for the coils are aligned radially intersecting at the origin (see Fig. 4). Let $d_i = r - r_i$ be the vector that points from the center of each coil to a point of interest $r \in \mathbb{R}^2$. As the coils are identical in their geometry and magnetic properties, it will be convenient to express the distance to each coil relative to one of the coils. This allows us to perform a fitting on one coil, and use a geometric transformation of this fitting for others. In particular, we use a coordinate system relative to the electromagnet placed in the positive y-axis (the "north" coil, where $i = 2$), such that

$$d_i^N = \mathrm{Rot}(\pi/2 - \theta_i)d_i = x_i\hat{i} + y_i\hat{j}, \tag{6}$$

where $\mathrm{Rot}(\theta)$ is the standard rotation matrix and N is used

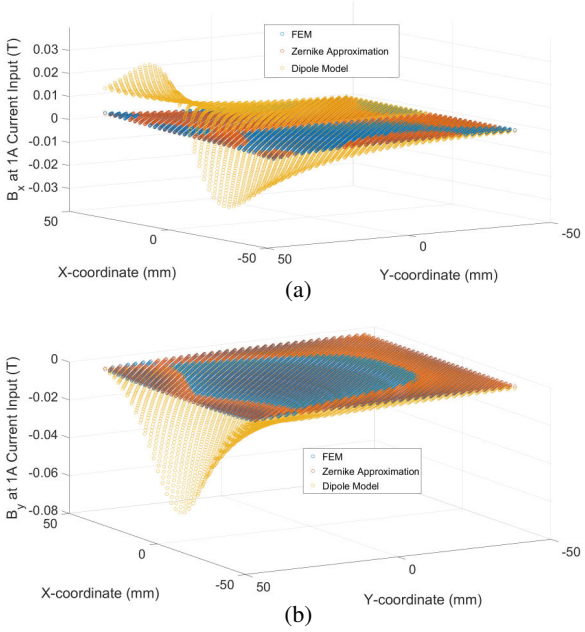

Fig. 3: Comparison of the (a) x- and (b) y-components of the magnetic field generated by a coil whose axis is parallel to the y-axis and center coordinates are $(0, 80\,\mathrm{mm})$.

to state that the north coil coordinates. Let $Z_x \in \mathbb{R}^\ell$ and $Z_y \in \mathbb{R}^\ell$, be a vector of basis functions to represent Zernike components used to fit the magnetic field generated by the north coil in x and y directions for a 1A input current, where

$$\begin{aligned} Z_x(d_i^N) &= \begin{bmatrix} 2x_iy_i \\ 3x_i^3 + 3x_iy_i^2 - 2x_i \\ x_i^3 - 3x_iy_i^2 \\ 4x_i^3y_i - 4x_iy_i^3 \end{bmatrix}, \\ Z_y(d_i^N) &= \begin{bmatrix} 1 \\ y_i \\ x_i^2 - y_i^2 \\ 3x_i^2y_i - y_i^3 \end{bmatrix}. \end{aligned} \tag{7}$$

Let $D_x \in \mathbb{R}^\ell$ and $D_y \in \mathbb{R}^\ell$ be a set of weights to combine the entries in $Z_x(d_i^N)$ and $Z_y(d_i^N)$, respectively, found by fitting the FEM data. The magnetic fields due to all m coils in the Cartesian (x and y) directions is thus given by

$$\begin{aligned} B_x &= \mu_0 \sum_{i=1}^{m} I_i(C^i_{N_{11}} Z_x(d_i^N)^T D_x + C^i_{N_{12}} Z_y(d_i^N)^T D_y), \\ B_y &= \mu_0 \sum_{i=1}^{m} I_i(C^i_{N_{21}} Z_x(d_i^N)^T D_x + C^i_{N_{22}} Z_y(d_i^N)^T D_y), \end{aligned} \tag{8}$$

where $C^i_{N_{jk}}$ is the jk^{th} component of the rotation matrix $C^i_N = \mathrm{Rot}(\theta_i - \pi/2)$, and I_i is the current in the i^{th} coil. The coefficients were obtained through non-linear least squares fit to the FEM data, yielding

$$\begin{aligned} D_x^{*T} &= \begin{bmatrix} 1.9038 & -0.0902 & -9.3645 & -17.0526 \end{bmatrix}, \\ D_y^{*T} &= \begin{bmatrix} -0.0094 & -0.1885 & 1.3961 & 3.8239 \end{bmatrix}. \end{aligned} \tag{9}$$

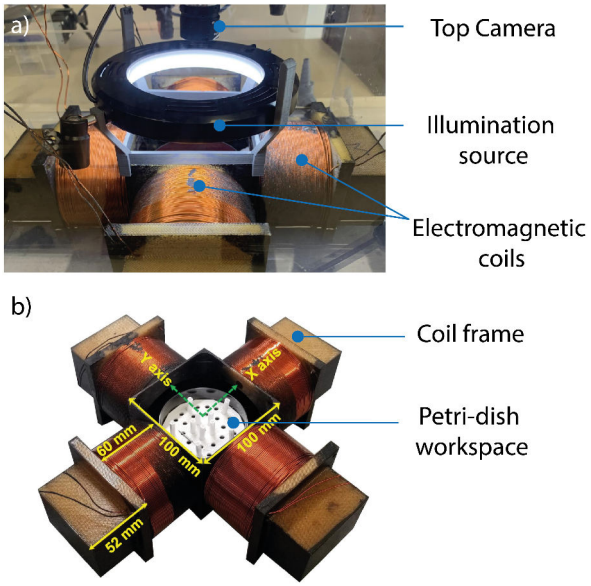

Fig. 4: MagnetoSuture™ Actuation System: a) Planar array of four electromagnets generate the desired magnetic field. An overhead camera is used for needle localization. b) A magnetic suture needle is submerged in a viscous solution in a Petri-dish placed at the center of the workspace.

Let the magnetic moment of the needle be

$$m_p = k_p h, \qquad k_p = \frac{\pi \rho_p^2 l_p B_p}{\mu_0}, \qquad h = \begin{bmatrix} \cos\theta \\ \sin\theta \end{bmatrix}. \tag{10}$$

The resultant torque produced on the needle is given by

$$\tau = k_p \mu_0 h^T S \begin{bmatrix} B_x \\ B_y \end{bmatrix}, \qquad S = \begin{bmatrix} 0 & 1 \\ -1 & 0 \end{bmatrix}. \tag{11}$$

The resultant force vector acting on the needle in x and y directions can be expressed as

$$F_x = -k_p h \begin{bmatrix} B_{xx} \\ B_{yx} \end{bmatrix}, \qquad F_y = -k_p h \begin{bmatrix} B_{xy} \\ B_{yy} \end{bmatrix}, \tag{12}$$

where, $B_{ab} = \partial B_a / \partial b$, which can be expressed in terms of the gradients for the north coil as

$$\begin{aligned} B_{xk} &= \sum_{i=1}^{m} I_i [C^i_{N_{11}} \partial_k Z_x (d_i^N)^T D_x + C^i_{N_{12}} \partial_k Z_y (d_i^N)^T D_y] \\ B_{yk} &= \sum_{i=1}^{m} I_i [C^i_{N_{21}} \partial_k Z_x (d_i^N)^T D_x + C^i_{N_{22}} \partial_k Z_y (d_i^N)^T D_y] \end{aligned} \tag{13}$$

where $k \in \{x, y\}$, and $\partial_k Z_a = \partial Z_a / \partial k$.

V. Needle Control Experiments

A. Experimental Setup

The experimental setup consists of four electromagnets orthogonally arranged along the X and Y axes, generating a magnetic object manipulation workspace that is 10 cm on a side. Specific details of the coil array, power apparatus, imaging methods, and needle localization techniques have been reported in our previous studies [26]–[28].

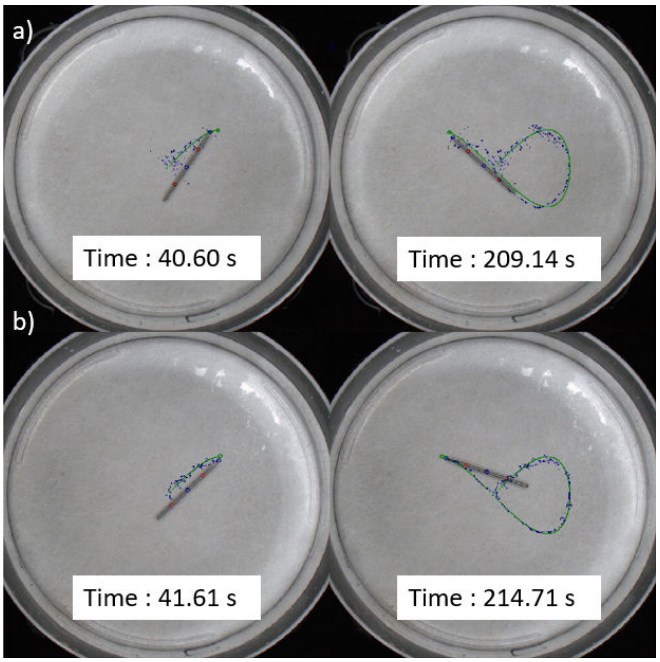

Fig. 5: Snapshots of real-time needle control at two different times for the reference path with: a) dipole, b) Zernike fit.

B. Needle Dynamics

As was done in [28], we assume the system is driftless, as sufficient damping ensures no motion occurs when the input currents are zero. Thus, we assume first order dynamics

$$\dot{r} = \frac{1}{c_t} F, \qquad \dot{\theta} = \frac{1}{c_r} \tau, \tag{14}$$

where the coefficients c_t and c_r map forces and torques to translational and rotational motion, obtained empirically to reduce the error for constant rate commands for each model.

The force to be applied to the needle should be constrained along its length. We impose a non-holonomic constraint on the needle's motion, as shown by the following equation

$$\begin{bmatrix} \dot{r} \\ \dot{\theta} \end{bmatrix} = \begin{bmatrix} \dfrac{hh^T F}{c_t} \\ \dfrac{\tau}{c_r} \end{bmatrix} = \begin{bmatrix} \cos\theta & 0 \\ \sin\theta & 0 \\ 0 & 1 \end{bmatrix} g(r,\theta) I = \begin{bmatrix} \cos\theta & 0 \\ \sin\theta & 0 \\ 0 & 1 \end{bmatrix} \begin{bmatrix} v \\ \omega \end{bmatrix}, \tag{15}$$

where the function $g(r, \theta)$ estimates the forces and torques generated from the magnetic field approximation model used. The magnetic field and its gradients are computed at two points along the length of the needle for improved accuracy.

C. Tip-Tracking Control

In many surgical procedures, such as suturing, the motion of the tip of the needle is of utmost importance, as it initiates

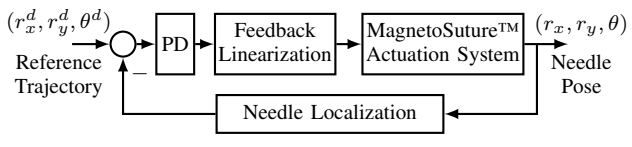

Fig. 6: Magnetic needle tip-tracking control scheme.

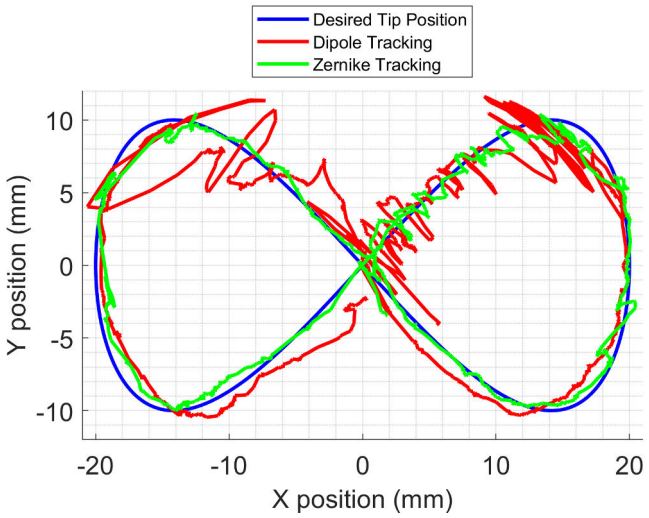

Fig. 7: Tip-tracking performance results for a lemniscate trajectory with the proposed Zernike fitting in comparison to the dipole model of magnetic field interaction.

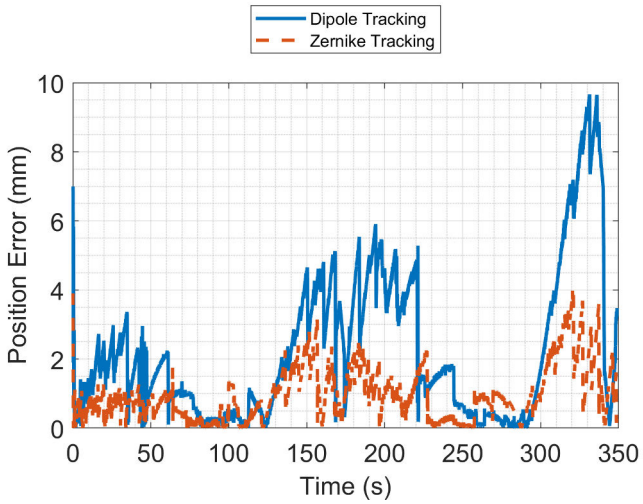

Fig. 8: Euclidean position error in the XY plane between the needle tip and reference lemniscate trajectory with dipole and proposed Zernike fit models of the magnetic field.

penetration into the tissue. Let $r_{tip}^T = [x_{tip}, y_{tip}]$ be the position of the tip and r the center of the needle, which is provided by the localization algorithm. As the needle is rigid, these are related as

$$r_{tip} = r + \frac{\lambda}{2}\begin{bmatrix}\cos\theta \\ \sin\theta\end{bmatrix} \tag{16}$$

where $\lambda = 23mm$ is the length of the needle. By differentiating these expressions, a unique mapping can be obtained between the tip velocity and the linear and angular velocities

$$\begin{bmatrix} v \\ \omega \end{bmatrix} = \begin{bmatrix} \cos\theta & \sin\theta \\ -\dfrac{1}{\lambda/2}\sin\theta & \dfrac{1}{\lambda/2}\cos\theta \end{bmatrix} \dot{r}_{tip}. \tag{17}$$

Given a differentiable desired reference path $r_{des}(t)$, we employ a PD control strategy to enable the tip tracking, i.e.,

$$\dot{r}_{tip} = k(r_{des}(t) - r_{tip}) + \dot{r}_{des}(t). \tag{18}$$

D. Motion Control Performance

In order to test the performance of needle tip tracking, we choose a time-based reference path, which starts at the center of the Petri-dish and traces a lemniscate trajectory. The desired reference point and reference speed are generated by the following equations in real-time

$$r_{des}(t) = \begin{bmatrix} a\,\sin(\frac{2\pi t}{T}) \\ a\,\sin(\frac{2\pi t}{T})\cos(\frac{2\pi t}{T}) \end{bmatrix} \tag{19}$$

where we set $a = 20mm$ and $T = 350s$.

We perform a lemniscate trajectory experiment for the dipole and Zernike fit models of the magnetic field. Fig. 5 shows snapshots at different time instances during these experiments. Fig. 7 shows the trajectories executed by the needle tip for both experiments. Fig. 8 presents how the Euclidean position error evolves during the tracking of the lemniscate trajectory for both the experiments. Fig. 9 shows the control inputs (coil currents) generated by the controller for both experiments. The RMS error while using the dipole and Zernike fit models to approximate the magnetic field are 2.35 mm and 1.71 mm, respectively.

It is important to note that the average computation times for the dipole and Zernike fit models (for the 4 coils combined) for an Acer Predator PH315-53, i7 10750H, RTX2060 CPU are around 9ms and 12ms, respectively. These times include computation at the two locations along the needle length.

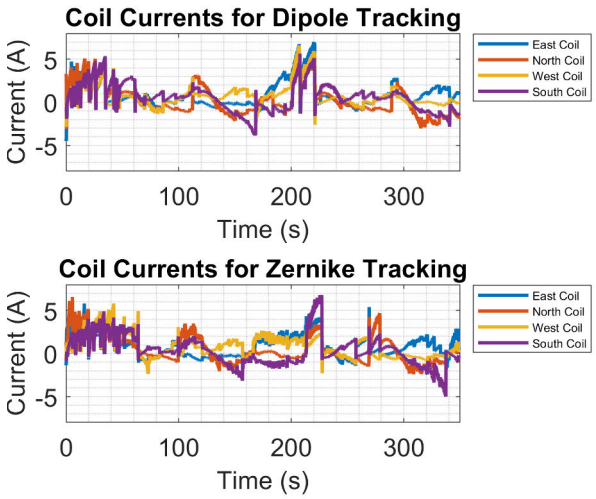

Fig. 9: Coil currents computed by the controller to track a lemniscate trajectory with a dipole model and the proposed Zernike fit of the magnetic field.

VI. Conclusions

We have presented improvements in control accuracy of a magnetic suture needle by using Zernike fit to obtain a more accurate model of the magnetic field generated by a coil array. At its best, there is an error reduction of 59% at time $t = 331s$, when the error drops from $9.66mm$ for the dipole model to $3.98mm$ for the Zernike fit model. On average, the error reduction is about 27%, as the RMS error is reduced from $2.35mm$ for the dipole model to $1.71mm$ for the Zernike fit model. The described method for fitting Zernike basis polynomials to a magnetic field may pave the way for more accurate control of magnetic agents, particularly in settings in which the agent is controlled near the coil where the dipole model exhibits large errors. Such control improvements may lead to improvements in minimally invasive surgery capabilities. Computation times for the magnetic field and gradients using dipole and Zernike models are minimal due to the closed-form analytic representation, which is crucial for real-time implementation. As the modeling makes individual fits for a given coil and because magnetic fields superimpose, the magnetic field approximation using the Zernike basis would also be applicable for 3D systems. This is left as the subject of future research.

References

[1] N. Simaan, R. M. Yasin, and L. Wang, "Medical technologies and challenges of robot-assisted minimally invasive intervention and diagnostics," *Annual Review of Control, Robotics, and Autonomous Systems*, vol. 1, no. 1, pp. 465–490, 2018.

[2] S. A. Antoniou, R. Pointner, and F. A. Granderath, "Single-incision laparoscopic cholecystectomy: A systematic review," *Surgical Endoscopy*, vol. 25, no. 2, pp. 367–377, 2011.

[3] R. S. Chamberlain and S. V. Sakpal, "A Comprehensive review of single-incision laparoscopic surgery (SILS) and natural orifice transluminal endoscopic surgery (NOTES) techniques for cholecystectomy," *Journal of Gastrointestinal Surgery*, vol. 13, no. 9, pp. 1733–1740, 2009.

[4] S. Maeso, M. Reza, J. A. Mayol, J. A. Blasco, M. Guerra, E. Andradas, and M. N. Plana, "Efficacy of the Da Vinci surgical system in abdominal surgery compared with that of laparoscopy: a systematic review and meta-analysis," *Annals of surgery*, vol. 252, no. 2, pp. 254–262, 2010.

[5] J. Rahmer, C. Stehning, and B. Gleich, "Remote magnetic actuation using a clinical scale system," *PLoS ONE*, vol. 13, no. 3, p. e0193546, 2018.

[6] J. J. Abbott, K. E. Peyer, M. C. Lagomarsino, L. Zhang, L. Dong, I. K. Kaliakatsos, and B. J. Nelson, "How should microrobots swim?" *The international journal of Robotics Research*, vol. 28, no. 11-12, pp. 1434–1447, 2009.

[7] Z. Yang and L. Zhang, "Magnetic actuation systems for miniature robots: A review," *Advanced Intelligent Systems*, vol. 2, no. 9, p. 2000082, 2020.

[8] J. Hwang, J.-y. Kim, and H. Choi, "A review of magnetic actuation systems and magnetically actuated guidewire-and catheter-based microrobots for vascular interventions," *Intelligent Service Robotics*, vol. 13, no. 1, pp. 1–14, 2020.

[9] M. Salehizadeh and E. Diller, "Three-dimensional independent control of multiple magnetic microrobots via inter-agent forces," *The International Journal of Robotics Research*, vol. 39, no. 12, pp. 1377–1396, 2020.

[10] M. P. Kummer, J. J. Abbott, B. E. Kratochvil, R. Borer, A. Sengul, and B. J. Nelson, "Octomag: An electromagnetic system for 5-dof wireless micromanipulation," *IEEE Transactions on Robotics*, vol. 26, no. 6, pp. 1006–1017, Dec 2010.

[11] O. Erin, M. Boyvat, J. Lazovic, M. E. Tiryaki, and M. Sitti, "Wireless mri-powered reversible orientation-locking capsule robot," *Advanced Science*, p. 2100463, 2021.

[12] J. Kim and S.-J. Kim, "A novel two-dimensional locomotion scheme of a micro-robot with only a uniform magnetic field," in *2014 IEEE International Conference on Robotics and Automation (ICRA)*. IEEE, 2014, pp. 2071–2076.

[13] J. Giltinan and M. Sitti, "Simultaneous six-degree-of-freedom control of a single-body magnetic microrobot," *IEEE Robotics and Automation Letters*, vol. 4, no. 2, pp. 508–514, 2019.

[14] A. J. Petruska, "Open-loop orientation control using dynamic magnetic fields," *IEEE Robotics and Automation Letters*, vol. 5, no. 4, pp. 5472–5476, 2020.

[15] F. Z. Temel, Ö. Erin, A. F. Tabak, and S. Yeşilyurt, "Bio-inspired micro robots swimming in channels," in *2012 Austrian Center of Competence in Mechatronics (ACCM)*. IEEE, 2012, pp. 6551–6557.

[16] J. W. Romanishin, K. Gilpin, and D. Rus, "M-blocks: Momentum-driven, magnetic modular robots," in *2013 IEEE/RSJ International Conference on Intelligent Robots and Systems*. IEEE, 2013, pp. 4288–4295.

[17] S. H. Kim and K. Ishiyama, "Magnetic robot and manipulation for active-locomotion with targeted drug release," *IEEE/ASME Transactions On Mechatronics*, vol. 19, no. 5, pp. 1651–1659, 2013.

[18] H.-W. Tung, K. E. Peyer, D. F. Sargent, and B. J. Nelson, "Noncontact manipulation using a transversely magnetized rolling robot," *Applied Physics Letters*, vol. 103, no. 11, p. 114101, 2013.

[19] D. C. Meeker, E. H. Maslen, R. C. Ritter, and F. M. Creighton, "Optimal realization of arbitrary forces in a magnetic stereotaxis system," *IEEE transactions on magnetics*, vol. 32, no. 2, pp. 320–328, 1996.

[20] K. B. Yesin, K. Vollmers, and B. J. Nelson, "Modeling and control of untethered biomicrorobots in a fluidic environment using electromagnetic fields," *The International Journal of Robotics Research*, vol. 25, no. 5-6, pp. 527–536, 2006.

[21] O. Erin, D. Antonelli, M. E. Tiryaki, and M. Sitti, "Towards 5-dof control of an untethered magnetic millirobot via MRI gradient coils," in *2020 IEEE International Conference on Robotics and Automation (ICRA)*. IEEE, 2020, pp. 6551–6557.

[22] A. J. Petruska, J. Edelmann, and B. J. Nelson, "Model-based calibration for magnetic manipulation," *IEEE Transactions on Magnetics*, vol. 53, no. 7, pp. 1–6, 2017.

[23] R. J. Noll, "Zernike polynomials and atmospheric turbulence," *JOsA*, vol. 66, no. 3, pp. 207–211, 1976.

[24] R. Lane and M. Tallon, "Wave-front reconstruction using a shack–hartmann sensor," *Applied optics*, vol. 31, no. 32, pp. 6902–6908, 1992.

[25] R. Marinică, C. S. Smith, and M. Verhaegen, "State feedback control with quadratic output for wavefront correction in adaptive optics," in *52nd IEEE Conference on Decision and Control*. IEEE, 2013, pp. 3475–3480.

[26] L. O. Mair, X. Liu, B. Dandamudi, K. Jain, S. Chowdhury, J. Weed, Y. Diaz-Mercado, I. N. Weinberg, and A. Krieger, "MagnetoSuture: Tetherless Manipulation of Suture Needles," *IEEE Transactions on Medical Robotics and Bionics*, vol. 2, no. 2, pp. 206–215, May 2020.

[27] M. Fan, X. Liu, K. Jain, D. Lerner, L. Mair, I. Weinberg, Y. Diaz-Mercado, and A. Krieger, "Towards autonomous control of magnetic suture needles," in *2020 IEEE/RSJ International Conference on Intelligent Robots and Systems (IROS)*, 10 2020, pp. 2935–2942.

[28] W. Pryor, Y. Barnoy, S. Raval, X. Liu, L. Mair, D. Lerner, O. Erin, G. D. Hager, Y. Diaz-Mercado, and A. Krieger, "Localization and control of magnetic suture needles in cluttered surgical site with blood and tissue," 2021.